Nondestructive Measurement of the Evolution of Layer-Specific Mechanical Properties in Sub-10 nm Bilayer Films

Kathleen M. Hoogeboom-Pot,*,[†] Emrah Turgut,[†] Jorge N. Hernandez-Charpak,[†] Justin M. Shaw,[‡] Henry C. Kapteyn,[†] Margaret M. Murnane,[†] and Damiano Nardi*,[†]

[†]JILA and Department of Physics, University of Colorado, Boulder, Colorado 80309-0440, United States
[‡]Electromagnetics Division, NIST, Boulder, Colorado 80305-3328, United States

S Supporting Information

ABSTRACT: We use short wavelength extreme ultraviolet light to independently measure the mechanical properties of disparate layers within a bilayer film for the first time, with single-monolayer sensitivity. We show that in Ni/Ta nanostructured systems, while their density ratio is not meaningfully changed from that expected in bulk, their elastic properties are significantly modified, where nickel softens while tantalum stiffens, relative to their bulk counterparts. In particular, the presence or absence of the Ta capping layer influences the mechanical properties of the Ni film. This nondestructive nanomechanical measurement technique represents the first approach to date able to distinguish the properties of composite materials well below 100 nm in thickness. This capability is critical for understanding and optimizing the strength, flexibility and reliability of materials in a host of nanostructured electronic, photovoltaic, and thermoelectric devices.

KEYWORDS: Ultrafast X-rays, nanometrology, nanomechanical properties, ultrathin films, monolayer sensitivity, photoacoustics
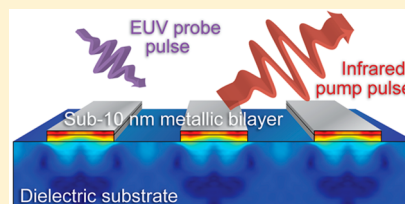
Tremendous progress in nanofabrication capabilities has made it possible to fabricate sub-10 nm structures and even single-atomic layers with high precision, enabling dramatic miniaturization of nanodevices. However, methods for characterizing the mechanical properties of ultrathin films and nanostructures are still severely limited at dimensions below 100 nm.[1] In recent years, extensions of visible probe metrology techniques, such as asynchronous optical samplings or visible light picosecond ultrasonics,[2,3] have pushed the sensitivity such that vertical breathing modes can be resolved in metallic films 5−15 nm in thickness.[3,4] Nonetheless, the fundamental diffraction limit of visible light probes prevents these techniques from resolving structured nanoscale systems, and moreover, the data analysis needed makes the study of composite films extremely challenging. This is a major challenge because the mechanical properties of thin films determine their strength, flexibility, and reliability in a host of nanostructured electronic, photovoltaic, and thermoelectric devices. Moreover, while a departure from bulk mechanical properties has long been expected and observed for nanoscale materials,[5,6] the precise mechanisms, magnitude, and even sign of these changes are still open questions,[7] which cannot be addressed without new approaches to nanoscale metrology.

Here we use short wavelength extreme ultraviolet (EUV) light to measure the mechanical properties of nanoscale Ta−Ni bilayers *with single-monolayer sensitivity* in a nondestructive measurement. By exciting a nanoscale grating using a femtosecond laser pulse, and probing the resulting acoustic waves and resonances using EUV beams, we can extract the density and elastic properties of sub-10 nm thin nickel (Ni) and tantalum (Ta) bilayers. To our knowledge this represents the

first work to distinguish the properties of two materials within bilayers below 100 nm in thickness. Using advanced frequency extraction methods, we can resolve shifts in acoustic frequencies below 1%. This ultrahigh sensitivity allows us to prove that although the density ratio of ultrathin Ta−Ni bilayer films is not significantly different from bulk, the few-nanometer films of Ni soften, while those of Ta stiffen, relative to their bulk counterparts. Finally, the presence or absence of the Ta capping layer further influences the effective properties of the Ni film.

To separate the mechanical properties of Ni and Ta components in the bilayers, we study a series of samples with varying layer thicknesses, as shown in Figure 1a. Using a calibrated sputtering process,[8] a 10 nm layer of Ni is first deposited on thermally oxidized Si substrates for all samples, followed by a Ta capping layer with thickness varying between 1 and 6 nm, to a precision of ≈0.1 nm (see Supporting Information). From multiple calibration measurements, the repeatability of the sputtering rates, and therefore thickness, were found to be better than 5%. The films are then patterned using optical lithography and subsequent ion milling to produce a periodic array of stripes that are 1 μm wide with a periodicity of 2 μm, that also serve as a diffraction grating for the EUV probe. To excite acoustic resonances in these gratings, we use a 25 fs laser pulse centered around 800 nm to induce impulsive thermal expansion. This results in both longitudinal cross-plane acoustic wave resonances (LAWs) in each wire, as well as
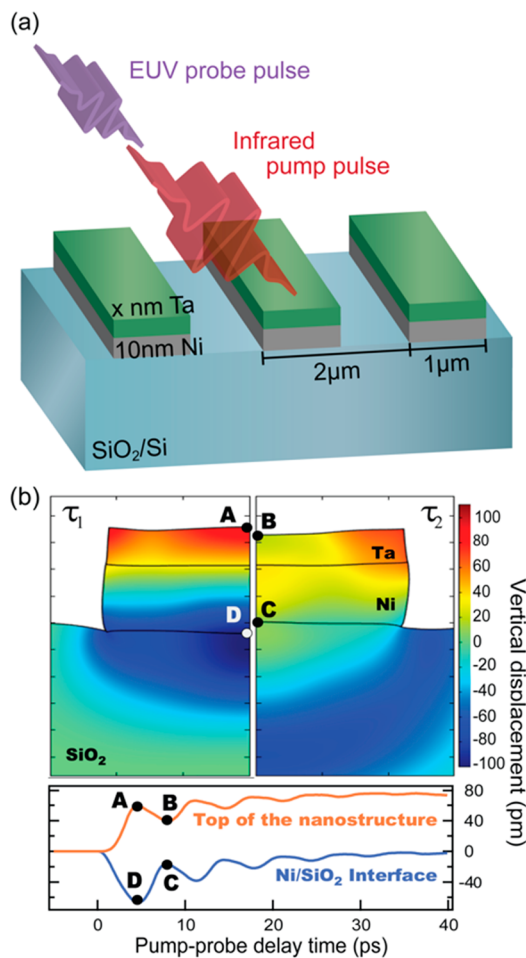
Figure 1. EUV acoustic nanometrology for extracting nanoscale mechanical properties. A series of Ni−Ta bilayers, with a constant Ni thickness of 10 nm and a Ta capping layer varying from 0 to 6 nm, are excited by an 800 nm pump pulse. The change in diffraction of the EUV probe beam is used to extract the mechanical properties of the bilayer. (b) Comparison of the displacement fields calculated by finite element analysis[17] at the peak (τ_1) and subsequent valley (τ_2) of the longitudinal acoustic oscillation clearly reveals the symmetric shape of the mode, placing antinodes at both the top surface and the interface with the substrate.

transverse surface acoustic standing-wave modes (SAWs) which are partially localized at the nanowires/substrate interface and radiating mechanical energy into the substrate due to the scattering with the grating.[9] The SAW wavelength is set by the periodicity of the grating (and its higher harmonics).[10,11] Analysis of these acoustic signals, as in Figure 1b, reveal the material properties of the individual ultrathin layers.

We use a time-delayed EUV high harmonic probe beam, with a wavelength centered at 30 nm, to detect the acoustic dynamics, along with the thermal expansion and relaxation of the bilayers.[12] In high harmonic generation (HHG), an intense femtosecond laser pulse is frequency upshifted using extreme nonlinear optics, to generate ultrafast coherent EUV and X-ray beams in a tabletop-scale apparatus.[13−15] The short-wavelength EUV probe beam diffracts from the periodic grating, and the change in diffraction efficiency (maximized by the 50% duty cycle configuration) is recorded as a function of the time delay between the laser pump and EUV probe pulse. The large wire width ensures that the longitudinal resonances we probe are

essentially those of the thin-film bilayers alone, while the periodic pattern gives a strong diffraction signal that enables ultrahigh sensitivity to displacements of the surface profile down to the picometer scale.[16]

The SAW velocity is exquisitely sensitive to the mass of any nanostructures deposited on the surface, particularly for high-frequency SAWs since their shorter wavelengths confine them to shallower substrate depths, where the wave velocity is most affected by any addition of mass.[18] Thus, each sample with a different Ta layer thickness (over the constant 10 nm of Ni) is expected to have a slightly different SAW velocity and oscillation frequency f_{SAW}. Indeed, Figure 2 demonstrates this behavior, which can be used to gauge the mass of the bilayer structure.

Combined with the volume change derived from the known change in thickness, this enables the first all-optical, non-destructive characterization of the density ratio between materials in ultrathin bilayers.

Specifically, as shown in Figure 2c, the SAW frequency decreases linearly with Ta thickness. Fitting this line yields values for two parameters: the slope γ, and intercept f_0. The relationship between f_{SAW} and Ta volume has slope $\alpha = \gamma/(Lz)$ where L and z are the width and length of the stripes, respectively. Then the relationship of f_{SAW} to wire mass must have slope $\beta = \alpha/\rho_{Ta}$ where ρ_{Ta} is the density of the Ta layers. Since we also know f_0 for when the mass of the wire is equal to the mass of the 10 nm layer of Ni alone m_{Ni}, $\beta = (f_0 - f_s)/m_{Ni}$ where f_s is the SAW frequency for the same wavelength propagating along the bare substrate surface. The frequency f_s must be known a priori, for example by using finite element analysis and literature properties for the materials comprising the substrate to identify the dominant excited modes.[11] Therefore,

$$\rho_{Ta} = \frac{\alpha}{\beta} = \frac{\gamma}{Lz}\frac{m_{Ni}}{f_0 - f_s} = \frac{\gamma}{Lz}\frac{\rho_{Ni}hLz}{f_0 - f_s} \quad (1)$$

where ρ_{Ni} and h are the density and thickness of the Ni layer, respectively. While the densities of the two materials in the bilayer cannot be independently determined in this way, the ratio between them can be found as

$$\frac{\rho_{Ta}}{\rho_{Ni}} = \frac{\gamma h}{f_0 - f_s} \quad (2)$$

Because of the large 2 μm period used here, the relatively long SAW wavelengths imply penetration depths well below the surface, and the SAW frequency shifts induced by the changing Ta mass are quite small: only ≈1%, or approximately 30 MHz, across the whole range of samples for the fundamental SAW order. To extract the SAW frequencies with sufficient precision to resolve this small change, we apply a chirp Z-transform[19] to obtain the frequency spectrum near the frequency peak, shown in Figure 2b. We then fit the peak to a Gaussian function to extract the central frequency. Averaging these peak values from many scans on the same sample results in the values reported in Figure 2c. The error bars represent the standard deviations of these measurements. This procedure yields frequency uncertainties of less than 0.5% for the fundamental SAW order and less than 2% for the higher orders. Linear fits to these data for each of the first four SAW harmonics, shown in Figure 2c, yield values for the Ta-to-Ni density ratio calculated according to eq 2, reported in Table 1. Note that each of the four orders generate consistent values for
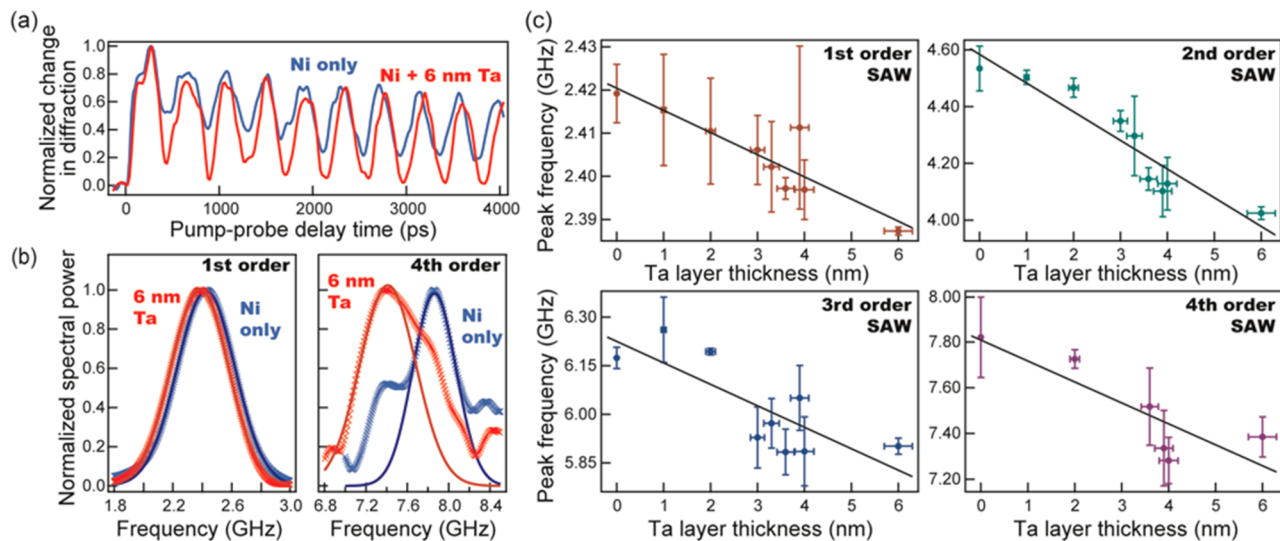
Figure 2. (a) The SAW frequency shift induced by adding 6 nm of Ta on top of 10 nm of Ni is clear in the raw diffraction signal. The additional mass slows the SAW propagation, lowering the oscillation frequency (red vs blue lines). (b) To extract small frequency shifts, we employ a chirp Z-transform to generate high-resolution spectra, plotted in crosses, near the resonance peaks. The fundamental and fourth-order peaks are shown. The center frequencies are extracted by Gaussian fits (solid lines). (c) The increasing Ta thickness from sample to sample results in a linear shift in the SAW frequency, visible in the first four SAW harmonic orders. The frequency shift is higher for higher orders because the shorter-wavelength SAW is confined closer to the surface, where the material is most affected by the extra mass in the bilayer structures. The linear fits to each data set are used to calculate the Ta-to-Ni density ratio.

Table 1. SAW Measurements Extracted from Four Harmonics Yield the Ta−Ni Density Ratio

	first order	second order	third order	fourth order
f_0 (GHz)	2.420 ± 0.007	4.584 ± 0.079	6.230 ± 0.033	7.810 ± 0.176
f_s (GHz)	2.447 ± 0.020	4.657 ± 0.020	6.614 ± 0.020	8.295 ± 0.020
γ (GHz/nm)	0.0051 ± 0.0009	-0.101 ± 0.014	-0.067 ± 0.019	-0.092 ± 0.028
ρ_{Ta}/ρ_{Ni}	1.93 ± 1.60	13.88 ± 10.1	1.70 ± 0.573	1.88 ± 0.722

the ratio, although that extracted from the second-order SAW data has a very large error bar. This value is likely more difficult to isolate precisely in our technique due to the 50% duty cycle employed for these samples and the resulting similarity in wavelength of the second SAW harmonic and the acoustic mode across the individual stripes, both of which contribute to the dynamic diffraction signal. Averaging the three similar values yields $\rho_{Ta}/\rho_{Ni} = 1.84 \pm 0.12$, which is statistically consistent with the ratio of the bulk material densities, 1.92.

Notably the slope is significantly higher for higher SAW harmonics due to the higher mass sensitivity enabled by shorter wavelengths. This illustrates that even greater precision for density measurements could be attained in EUV acoustic metrology simply by using gratings with shorter periodicity.

While the SAW dynamics dominate changes in the EUV diffraction signal over many nanoseconds, resonant longitudinal cross-plane acoustic oscillations in the bilayers themselves are visible during the first 20 ps following excitation by the pump pulse,[20] as shown in Figure 3. The frequency shifts significantly as the Ta thickness is varied with sensitivity at the monolayer level. Furthermore, by comparing three identical Ni/Ta film samples etched for different amounts of time, we verify that the resonant frequencies we measure are not affected by potential overetching of the stripe pattern into the substrate. This ensures that the shifts we observe are uniquely related to the changing Ta thickness.

The fast decay of the LAW oscillations makes a simple Fourier transform (which assumes stationary oscillations) inappropriate for extracting the resonant frequencies. Instead
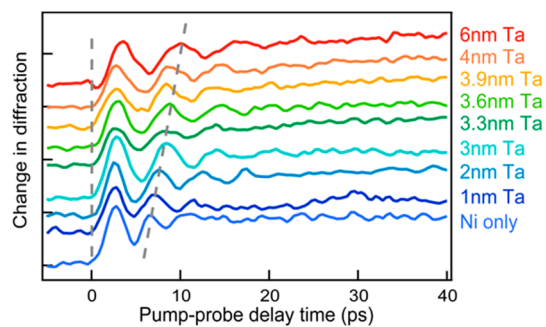

Figure 3. (a) Increasing the Ta thickness from sample to sample results in a shift in the resonant LAW frequencies of the bilayers themselves, with sensitivity at the monolayer level. The dashed lines serve as guides to the eye, marking time-zero and the shifting location of the second oscillation maximum.

we employ the matrix pencil method (MPM), which projects a function onto the set of exponentials with complex exponents to a specified precision limit, allowing it to reliably capture both oscillation frequencies and damping rates of the signal components isolated from the noise inherent to experimental data.[21−23] In this way we extract the set of oscillation periods shown in Figure 4, with uncertainties less than 0.7%. The resonant frequencies of a bilayer can be calculated by enforcing the condition that (displacement, stress) = $(u, 0)$ be an eigenvector of the appropriate acoustic transfer matrix (stress-
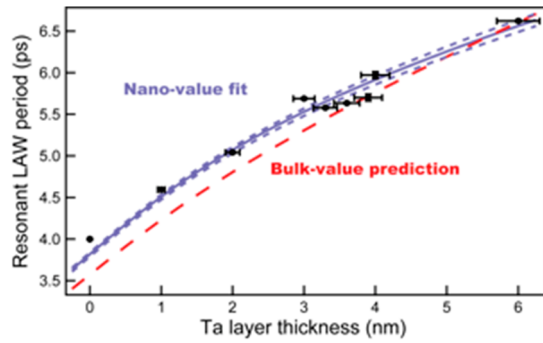
Figure 4. Resonant LAW periods of the bilayer structures extracted by using MPM clearly are not well matched by predictions using bulk material parameters (dashed red). Instead, a least-squares optimization algorithm fits the data in order to extract the effective nanoscale longitudinal velocities of the Ni and Ta layers. This fit is plotted in solid blue, while the dashed blue lines mark the fits to the diagonal extremes of the error bars and indicate the upper and lower bounds of the extracted effective velocities. The very small vertical error bars on the data represent the variation in the MPM-extracted periods. The horizontal error bars represent the 5% uncertainty in layer thickness resulting from the calibrated sputtering deposition process.

free boundary condition) as in calculating the localized surface modes of a semi-infinite superlattice.[5]

In our case, where the SiO_2 substrate has lower acoustic impedance than the Ni layer, the resonant modes will be analogous to organ-pipe modes with two open ends (see Figure 1b); i.e., the resonant frequencies will be the same as those for an unsupported bilayer membrane[24] and can be calculated by enforcing the eigenvector condition for a transfer matrix corresponding to one-way propagation across the Ta and Ni layers. This transfer matrix is given by

$$\tau = \begin{pmatrix} \cos(q_{Ni} d_{Ni}) & \sin(q_{Ni} d_{Ni})/\omega Z_{Ni} \\ -\omega Z_{Ni} \sin(q_{Ni} d_{Ni}) & \cos(q_{Ni} d_{Ni}) \end{pmatrix}$$
$$\times \begin{pmatrix} \cos(q_{Ta} d_{Ta}) & \sin(q_{Ta} d_{Ta})/\omega Z_{Ta} \\ -\omega Z_{Ta} \sin(q_{Ta} d_{Ta}) & \cos(q_{Ta} d_{Ta}) \end{pmatrix} \quad (3)$$

where ω is the LAW angular frequency, d_x is the thickness of the respective layers, Z_x is the acoustic impedance ($Z_x = \rho_x v_x$ for LAW velocity v_x), and $q_x = \omega/v_x$. We require

$$\tau \begin{pmatrix} u \\ 0 \end{pmatrix} = \lambda \begin{pmatrix} u \\ 0 \end{pmatrix} \quad (4)$$

for any scalar eigenvalue λ. The second component of this matrix equation implies that resonant frequencies will solve the transcendental equation

$$\tan\left(\frac{\omega d_{Ni}}{v_{Ni}}\right) + Z_{Ta}/Z_{Ni} \tan\left(\frac{\omega d_{Ta}}{v_{Ta}}\right) = 0 \quad (5)$$

Note that although these equations dramatically simplify in the long-wavelength limit ($q_x d_x \to 0$), this cannot be applied to our case where the wavelength of the open-pipe resonant mode is only twice the total thickness of the bilayer. Furthermore, we confirmed that the full transfer matrix approach is the only one able to reliably predict the resonant frequencies extracted by the matrix pencil method using finite element models. This approach contrasts with other models that might ignore the influence of a boundary, such as treating a bilayer as a single

material with elastic properties corresponding to the linear average of the component layers. Our simulated frequencies match the predictions of the open-pipe formulas employed in our analysis across a wide range of acoustic mismatch between the bilayer and substrate. As shown by the red dashed line in Figure 4, the resonant periods predicted using bulk material properties clearly fail to match those we observe as the Ta layer thickness is varied. Before analyzing the data further to understand how layer properties may deviate from those of bulk materials, it is important to consider how the presence of the typical tantalum pentoxide layer on Ta would affect our measurements. Since every nanometer of Ta_2O_5 that forms consumes approximately 0.4 nm of Ta, we compare simulated dynamics of the Ni/Ta bilayer with nominal thicknesses to those of a $Ni/Ta/Ta_2O_5$ system with nominal Ni thickness and nominal Ta thickness minus 0.4 nm per nanometer of added oxide. Given the literature values of all material properties, we find that the resonant frequencies from the two simulations are the same within experimental error bars. This finding can be explained by the fact that the presence of any thin (<0.5−1 nm) oxide layer is essentially compensated by the Ta loss, so that it is reasonable to conduct our analysis assuming the nominal Ni and Ta thicknesses and no oxide.

Therefore, we conclude that the discrepancy between the observed resonant periods and those predicted by bulk material properties can be attributed primarily to changes in the elastic properties of the ultrathin layers. We use v_{Ni} and v_{Ta} as our only fit parameters in a least-squares optimization algorithm using eq 5 to find the effective nanolayer velocities that provide the best fit to the data. However, we find that the point from the Ni-only sample (at Ta thickness = 0 nm) must be excluded to achieve a good fit to the rest of the data. The blue solid line in Figure 4 displays the result, while the blue dotted lines mark the outer bounds determined by fitting the diagonal extremes of the error bars on each data point. These fits indicate the effective nanoscale $v_{Ni} = 5240 + 40/−30$ m/s and $v_{Ta} = 5180 + 150/−170$ m/s. These values are significantly different from the bulk values, $v_{Ni,bulk} = 5600$ m/s and $v_{Ta,bulk} = 4100$ m/s.[25] Moreover, the best-fit v_{Ni} is indeed significantly different from the value associated with the Ni-only resonant period, $v_{Ni,only} = 5000 \pm 10$ m/s. This implies both that the 10 nm layer of Ni has different elasticity from that expected for a bulk material and that it is further modified by the addition of the Ta layer. Moreover, the two layers deviate from their bulk counterparts in opposite ways. We note that there is no significant intermixing or alloying between the two materials beyond ≈0.5 nm around the interface, since independent measurements on similar samples show that the magnetic properties of the Ni layer match those of pure Ni,[26] allowing us to discard intermixing as a possible cause of the observed behaviors.

Fitting the data in this way presumes that the elastic properties of Ni and Ta are constant across the entire set of samples. While this is a reasonable assumption for the constant 10 nm layer of Ni, one could argue the Ta layer may well behave differently at a 1 nm thickness than for 6 nm. Given the lower sensitivity of the measured oscillation periods to the Ta velocity in the thinnest layers we examine, we can neither confirm nor rule out this possibility. Our set of measured periods would be consistent with an effective velocity in Ta that varies from 5000 m/s at 6 nm to about 6000 m/s for <3 nm.

A number of mechanisms for nanoscale elastic changes in films and superlattices have been proposed, with disparate trends and magnitudes. For example, the atomic layers near a

surface will exhibit different elastic constants than those deep within the bulk volume. This causes a larger portion of the free energy of the film to be surface energy, having effects that cannot be ignored in reduced geometries.[27] However, the surface elastic constants calculated by Shenoy[28] using these principles suggest a change that is at least an order of magnitude smaller than we observe. Interface layers and bonding across them will also influence the effective elastic constants we extract. In particular, the fact that the ultrathin Ni layer alone behaves differently than the Ni layers under Ta lends evidence to the importance of these effects. Lattice mismatch between different materials and residual stress influence free energy surface-to-volume ratios in thin films. This has been used to explain some changes in elasticity, comparable to those we observe, in the softening of Si thin films on SiO_2 substrate.[29] However, the trends predicted by more rigorous models[30,31] do not account for what we or Fedorchenko et al.[29] observe. Softening due to a weak interfacial bond or equivalently interface layers with different properties than a bulk-like core was modeled by Rossignol et al.,[8] but notably their single parameter describing the displacement discontinuity across the interface does not allow enough freedom to fit our data if either bulk velocities, or $v_{Ni,only}$ and the best-fit v_{Ta} are assumed. Ultrathin films are also prone to large volume fractions of defects or soft intergrain areas between small grains.[20,32,33] Stiffening in layers as thick as those we study is less often observed, but it has typically been attributed to strain-induced changes in third-order elasticity.[3,20,34,35] In particular, Ogi et al.[3] observe a correlation between measured out-of-plane strain and the stiffening of sub-10 nm Pt and Fe films. However, to our knowledge, changes of the magnitude exhibited by our Ta layers have not been previously observed in metallic films.

It is likely that a combination of effects that are inherently due to the dimensionality of the materials, some lattice deformation from the interfaces between different materials, and fabrication conditions contribute to the changes in elastic properties that we observe. Further characterization using multiple techniques to analyze film microstructure (as with transmission electron microscopy − TEM) and lattice strain (as with X-ray diffraction − XRD), as well as exploration of how fabrication techniques (for example, sputtering vs atomic layer deposition − ALD) and conditions (such as thermally cycling the film to impose different values of residual stress in the samples) affect the elasticity changes, could illuminate more of the specific mechanisms involved. Exciting multiple LAW resonances in the bilayers[36] could also reveal more about the importance of changes localized around interfaces.[20]

In conclusion, we employed the first demonstration of EUV-based SAW mass sensing to show that the Ta-to-Ni density ratio in sub-10 nm bilayer films is not significantly changed from that expected in bulk materials. However, their elastic properties are significantly modified. In particular, we observe that, within the same bilayer, the ultrathin films of Ni and Ta soften and stiffen relative to their bulk counterparts, respectively. Finally, the presence or absence of the Ta capping layer further influences the effective properties of the Ni layer. This work presents the first combined measurement of elastic properties in ultrathin layers with mass-sensing capabilities to date and also represents the first work to date to distinguish the properties of two materials within bilayers below 100 nm in thickness. This allows accurate assessment of nanoscale material properties, which govern their strength, flexibility, and reliability

in a host of nanostructured electronic, photovoltaic, and thermoelectric devices.

■ ASSOCIATED CONTENT

ⓢ Supporting Information

The Supporting Information is available free of charge on the ACS Publications website at DOI: 10.1021/acs.nano-lett.6b00606.

> It includes more detailed descriptions of the fabrication process, calibration procedure, and XRR measurements (PDF)

■ AUTHOR INFORMATION

Corresponding Authors
*E-mail: hoogeboo@colorado.edu.
*E-mail: damiano.nardi@jila.colorado.edu.

Notes
The authors declare no competing financial interest.

■ REFERENCES

(1) King, S. W.; Simka, H.; Herr, D.; Akinaga, H.; Garner, M. Research Updates: The three M's (materials, metrology, and modeling) together pave the path to future nanoelectronic technologies. *APL Mater.* **2013**, *1*, 040701.

(2) Bartels, A.; Cerna, R.; Kistner, C.; Thoma, A.; Hudert, F.; Janke, C.; Dekorsy, T. Ultrafast time-domain spectroscopy based on high-speed asynchronous optical sampling. *Rev. Sci. Instrum.* **2007**, *78*, 035107.

(3) Ogi, H.; Fujii, M.; Nakamura, N.; Shagawa, T.; Hirao, M. Resonance acoustic-phonon spectroscopy for studying elasticity of ultrathin films. *Appl. Phys. Lett.* **2007**, *90*, 191906.

(4) Peli, S.; Cavaliere, E.; Benetti, G.; Gandolfi, M.; Chiodi, M.; Cancellieri, C.; Giannetti, C.; Ferrini, G.; Gavioli, L.; Banfi, F. Mechanical properties of Ag nanoparticle thin films synthesized by supersonic cluster beam deposition. *J. Phys. Chem. C* **2016**, *120*, 4673−4681.

(5) Cammarata, R. C.; Sieradzki, K. Effects of surface stress on the elastic moduli of thin films and superlattices. *Phys. Rev. Lett.* **1989**, *62*, 2005.

(6) Yang, W. M. C.; Tsakalakos, T.; Hilliard, J. E. Enhanced elastic modulus in composition-modulated gold-nickel and copper-palladium foils. *J. Appl. Phys.* **1977**, *48*, 876−879.

(7) Chang, I. L.; Chang, S. H.; Huang, J. C. The theoretical model of fcc ultrathin film. *Int. J. Solids Struct.* **2007**, *44*, 5818−5828.

(8) Rossignol, C.; Perrin, B.; Bonello, B.; Djemia, P.; Moch, P.; Hurdequint, H. Elastic properties of ultrathin permalloy/alumina multilayer films using picosecond ultrasonics and Brillouin light scattering. *Phys. Rev. B: Condens. Matter Mater. Phys.* **2004**, *70*, 094102.

(9) Nardi, D.; Travagliati, M.; Siemens, M. E.; Li, Q.; Murnane, M. M.; Kapteyn, H. C.; Ferrini, G.; Parmigiani, F.; Banfi, F. Probing thermomechanics at the nanoscale: impulsively excited pseudosurface acoustic waves in hypersonic phononic crystals. *Nano Lett.* **2011**, *11*, 4126−4133.

(10) Nardi, D.; Hoogeboom-Pot, K. M.; Hernandez-Charpak, J. N.; Tripp, M.; King, S. W.; Anderson, E. H.; Murnane, M. M.; Kapteyn, H.

C. Probing limits of acoustic nanometrology using coherent extreme ultraviolet light. *Proc. SPIE* **2013**, *8681*, 86810N.

(11) Nardi, D.; Banfi, F.; Giannetti, C.; Revaz, B.; Ferrini, G.; Parmigiani, F. Pseudosurface acoustic waves in hypersonic surface phononic crystals. *Phys. Rev. B: Condens. Matter Mater. Phys.* **2009**, *80*, 104119.

(12) Hoogeboom-Pot, K. M.; Hernandez-Charpak, J. N.; Gu, X.; Frazer, T. D.; Anderson, E. H.; Chao, W.; Falcone, R. W.; Yang, R.; Murnane, M. M.; Kapteyn, H. C.; Nardi, D. A new regime of nanoscale thermal transport: Collective diffusion increases dissipation efficiency. *Proc. Natl. Acad. Sci. U. S. A.* **2015**, *112*, 4846−4851.

(13) Rundquist, A.; Durfee, C. G.; Chang, Z.; Herne, C.; Backus, S.; Murnane, M. M.; Kapteyn, H. C. Phase-matched generation of coherent soft X-rays. *Science* **1998**, *280*, 1412−1415.

(14) Popmintchev, T.; Chen, M. C.; Popmintchev, D.; Arpin, P.; Brown, S.; Alisauskas, S.; Andriukaitis, G.; Balciunas, T.; Mucke, O. D.; Pugzlys, A.; Baltuska, A.; Shim, B.; Schrauth, S.; Gaeta, A.; Hernandez-Garcia, C.; Plaja, L.; Becker, A.; Jaron-Becker, A.; Murnane, M. M.; Kapteyn, H. C. Bright coherent ultrahigh harmonics in the keV x-ray regime from mid-infrared femtosecond lasers. *Science* **2012**, *336*, 1287−1291.

(15) Miao, J.; Ishikawa, T.; Robinson, I. K.; Murnane, M. M. Beyond crystallography: Diffractive imaging using coherent x-ray light sources. *Science* **2015**, *348*, 530−535.

(16) Tobey, R. I.; Siemens, M. E.; Cohen, O.; Murnane, M. M.; Kapteyn, H. C.; Nelson, K. A. Ultrafast extreme ultraviolet holography: dynamic monitoring of surface deformation. *Opt. Lett.* **2007**, *32*, 286−288.

(17) COMSOL Inc. *COMSOL Multiphysics, Version 4.3b*; COMSOL, Inc.: Burlington, MA, 2013.

(18) Nardi, D.; Zagato, E.; Ferrini, G.; Giannetti, C.; Banfi, F. Design of a surface acoustic wave mass sensor in the 100 GHz range. *Appl. Phys. Lett.* **2012**, *100*, 253106.

(19) Rabiner, L.; Schafer, R.; Rader, C. The chirp z-transform algorithm. *IEEE Trans. Audio Electroacoust.* **1969**, *17*, 86−92.

(20) Ogi, H.; Nakamura, N.; Hirao, M. Picosecond ultrasound spectroscopy for studying elastic modulus of thin films: a review. *Nondestr. Test. Eval.* **2011**, *26*, 267−280.

(21) Hua, Y.; Sarkar, T. K. Matrix pencil method for estimating parameters of exponentially damped/undamped sinusoids in noise. *IEEE Trans. Acoust., Speech, Signal Process.* **1990**, *38*, 814−824.

(22) Sarkar, T. K.; Pereira, O. Using the matrix pencil method to estimate the parameters of a sum of complex exponentials. *IEEE Antennas and Propagation Mag.* **1995**, *37*, 48−55.

(23) Fernandez del Rio, J. E.; Sarkar, T. K. Comparison between the matrix pencil method and the Fourier transform technique for high-resolution spectral estimation. *Digit. Signal Process.* **1996**, *6*, 108−125.

(24) Groenen, J.; Poinsotte, F.; Zwick, A.; Sotomayor Torres, C. M.; Prunnila, M.; Ahopelto, J. Inelastic light scattering by longitudinal acoustic phonons in thin silicon layers: From membranes to silicon-on-insulator structures. *Phys. Rev. B: Condens. Matter Mater. Phys.* **2008**, *77*, 045420.

(25) Table of Acoustic Properties of Solids. Onda Corporation. http://www.ondacorp.com/images/Solids.pdf (accessed July 15, 2015).

(26) La-O-Vorakiat, C.; Turgut, E.; Teale, C. A.; Kapteyn, H. C.; Murnane, M. M.; Mathias, S.; Aeschlimann, M.; Schneider, C. M.; Shaw, J. M.; Nembach, H. T.; Silva, T. J. Ultrafast Demagnetization Measurements using Extreme Ultraviolet Light: Comparison of Electronic and Magnetic Contributions. *Phys. Rev. X* **2012**, *2*, 011005.

(27) Miller, R. E.; Shenoy, V. B. Size-dependent elastic properties of nanosized structural elements. *Nanotechnology* **2000**, *11*, 139−147.

(28) Shenoy, V. B. Atomistic calculations of elastic properties of metallic fcc crystal surfaces. *Phys. Rev. B: Condens. Matter Mater. Phys.* **2005**, *71*, 094104.

(29) Fedorchenko, A. I.; Wang, A. B.; Cheng, H. H. Thickness dependence of nanofilm elastic modulus. *Appl. Phys. Lett.* **2009**, *94*, 152111.

(30) Nakamura, N.; Ogi, H.; Yasui, T.; Fujii, M.; Hirao, M. Mechanism of elastic softening behavior in a superlattice. *Phys. Rev. Lett.* **2007**, *99*, 035502.

(31) Clemens, B. M.; Eesley, G. L. Relationship between interfacial strain and the elastic response of multilayer metal films. *Phys. Rev. Lett.* **1988**, *61*, 2356.

(32) Nakamura, N.; Uranishi, A.; Wakita, M.; Ogi, H.; Hirao, M.; Nishiyama, M. Elastic stiffness of $L1_0$ FePt thin film studied by picosecond ultrasonics. *Appl. Phys. Lett.* **2011**, *98*, 101911.

(33) Karanikas, J. M.; Sooryakumar, R.; Phillips, J. M. Dispersion of elastic waves in supported CaF_2 films. *J. Appl. Phys.* **1989**, *65*, 3407−3410.

(34) Nakamura, N.; Uranishi, A.; Shagawa, T.; Ogi, H.; Hirao, M.; Nishiyama, M. Laser-Induced Coherent Acoustic Phonons for Measuring Elastic Constants of Ultra-Thin Films. *J. Solid Mech. Mater. Eng.* **2008**, *2*, 1420−1426.

(35) Lee, Y. C.; Bretz, K. C.; Wise, F. W.; Sachse, W. Picosecond acoustic measurements of longitudinal wave velocity of submicron polymer films. *Appl. Phys. Lett.* **1996**, *69*, 1692−1694.

(36) Li, Q.; Hoogeboom-Pot, K. M.; Nardi, D.; Murnane, M. M.; Kapteyn, H. C.; Siemens, M. E.; Anderson, E. H.; Hellwig, O.; Dobisz, E.; Gurney, B.; Yang, R.; Nelson, K. A. Generation and control of ultrashort-wavelength two-dimensional surface acoustic waves at nanoscale interfaces. *Phys. Rev. B: Condens. Matter Mater. Phys.* **2012**, *85*, 195431.